

Multiple ionization of Ar, Kr, and Xe in a superstrong laser field

Aleksei S. Kornev,^{*} Elena B. Tulenko, and Boris A. Zon

Voronezh State University, Voronezh, Russia

(Received 4 October 2011; published 21 November 2011)

We report the numerical calculation of $\text{Ar}^{9+} \dots \text{Ar}^{13+}$, $\text{Kr}^{13+} \dots \text{Kr}^{17+}$, and $\text{Xe}^{19+} \dots \text{Xe}^{23+}$ ion yield in the laser field with intensity exceeding 10^{19} W/cm². The results of the calculations agree with the experimental data [K. Yamakawa *et al.*, *Phys. Rev. A* **68**, 065403 (2003)] (for the Ar ions) or qualitatively (for the Kr ions). The theoretical results disagree with the experimental data for the Xe ions. We discuss the possible influence of the relativistic effects on this disagreement between theory and experiment. We obtained the approximation formula for the position of the maximum ionic population with the given ionization multiplicity Z depending on the radiation intensity. This position is described by the power function of Z ; the exponent is determined by the dependence of sequential ionization potentials on Z value. We discuss the dependence of the approximation formula parameters on the value of the FWHM of the laser pulse.

DOI: [10.1103/PhysRevA.84.053424](https://doi.org/10.1103/PhysRevA.84.053424)

PACS number(s): 32.80.Fb

I. INTRODUCTION

In recent years, the formation of multiply charged atomic ions (MCI's) in a superstrong laser field with an intensity up to 10^{19} W/cm² has been actively studied in experiments [1–12]. In Refs. [3,5] multiply charged Xe^{23+} ions which are record-breaking for the optical frequency fields have been obtained, and in Ref. [11] Xe^{24+} ions have been obtained.

Superstrong laser radiation has attracted increased interest due to the manifestation of the relativistic effects in these fields [13]. The first emergent relativistic effect is connected with the influence of the magnetic component of the laser radiation light field on a free electron motion. The trajectory of the free electron motion is distorted under the influence of the magnetic field. Therefore, the rescattering processes that were connected with the returning of the electron to the parent ion and were of importance in the formation of the multiply charged ions in linearly polarized fields with less intensity [14] lose their importance now. Experimental verification of the rescattering suppression due to relativistic effects at ionization multiplicity higher than 8 was noted in Refs. [1,2,5] and was examined in Ref. [4]. As the rescattering process ceases to dominate, the formation of the multiply charged ions occurs due to the direct laser field impact on atoms or ions.

Single ionization is described well by the Ammosov-Delone-Krainov (ADK) model [15–18], which is substantially single-body. References [19,20] are devoted to the relativistic generalization of this model. However, the probabilities of multiply charged ion formation are described poorly by the ADK model. We have developed the many-body theory of tunnel ionization earlier in Refs. [21–26]. Within the framework of this theory, it has been shown that for the ions of multiplicity 2 and higher the inelastic tunnel effect (ITE) appears to be quite essential, allowing to take into account the filling of the ion excited states within the intermediate stages of the process [23,24]. In the fields with FWHM less than 5 fs, the collective tunnel effect can become dominant

when some electrons are removed from an atom or an ion simultaneously [25,26].

In Refs. [25,26], general expressions are presented for the rate of the many-body tunnel ionization of ions with regard to the p and d shells of atoms and ions, and the solution method of the appropriate kinetic equations is stated. Herewith inelastic and collective tunnel effects, as well as the fast relaxation of magnetic quantum numbers of electrons due to spin-orbit interaction (m relaxation) [6], have been taken into account. The aim of this work is the comparison of the results obtained within the framework of the many-body theory with the experimental data from Refs. [3,5], where the formation of $\text{Ar}^{9+} \dots \text{Ar}^{16+}$, $\text{Kr}^{13+} \dots \text{Kr}^{19+}$, and $\text{Xe}^{17+} \dots \text{Xe}^{23+}$ MCI's by the linearly polarized pulse with the central wavelength 800 nm and the FWHM 25 fs is investigated. The results of the calculations and comparison with the experiment are given in Sec. II.

In Sec. III the approximation formula for describing the position of the maximum of the formation probability of the ions with the specified multiplicity Z depending on the radiation intensity is derived. The existence of this maximum is due to the competition of the process of increasing the number of the multiplicity Z ions, formed from the ions with less multiplicity ($Z - 1$), and that of decreasing their number due to the formation of the ions with higher multiplicity ($Z + 1$). A similar approximation formula was proposed in a recent paper [12]; its accuracy, however, is not sufficiently high, as is demonstrated in Sec. III.

The atomic units ($\hbar = m_e = e = 1$) are used hereafter, except in specified cases.

II. KINETIC EQUATIONS

According to Refs. [23–26], the formation of multiply charged ions due to the tunnel effect is a multichannel cascading process. In conditions of the experiments from Refs. [3,5] it includes single-electron tunnel cascading transitions which can be accompanied by ionic core excitation.

Multiple ionization of neutral atoms in the tunnel mode by a laser pulse is described by the set of the kinetic equations for

^{*}a-kornev@yandex.ru

the populations of various ionic states C_f [23],

$$\frac{dC_f}{dt} = \sum_{f'=0}^{f-1} W_{f \rightarrow f'}(t) C_{f'} - \sum_{f'=f+1}^{f_{\text{tot}}} W_{f' \rightarrow f}(t) C_{f'}, \quad (1)$$

$$f = 0, 1, \dots, f_{\text{tot}},$$

$$C_0(-\infty) = 1, \quad C_1(-\infty) = \dots = C_{f_{\text{tot}}}(-\infty) = 0. \quad (2)$$

Indices f, f' in Eqs. (1) enumerate the ionic states. $W_{f' \rightarrow f}(t)$ is the rate of tunnel transition from state $|f'\rangle$ to state $|f\rangle$ taking into account the laser field F nonmonochromaticity by introducing the pulse envelope $F(t)$. Equations similar to (1) have been used in a recent study [30] to describe multiple ionization by free electron laser radiation.

In order to obtain the explicit form of $W_{f' \rightarrow f}(t)$, the appropriate rate of tunneling in the monochromatic linearly polarized laser field with the amplitude F [25] is taken as the basis:

$$W_{klm}(F) = \sqrt{\frac{6}{\pi}} \frac{(2l+1)(l+m)!}{2^{m+1}m!(l-m)!} C_{kl}^2 Q^2 \kappa^2 \times \left(\frac{2F_a}{F}\right)^{2\nu-m-\frac{3}{2}} \exp\left(-\frac{2F_a}{3F}\right). \quad (3)$$

Here, l and m are the orbital and magnetic quantum numbers of the electron, respectively:

$$\kappa = \sqrt{2E_j}, \quad E_j = E_j^{(0)} + \Delta_j, \quad F_a = \kappa^3, \quad \nu = Z/\kappa,$$

$E_j^{(0)}$ is the j th ionization potential of the parental atom or ion, Δ_j is the energy of the core excitation, F_a is the residual ion electric field strength on the Bohr orbit, Z is the charge of the residual ion, and Q is the overlap integral. The dimensionless constant C_{kl} in expression (3) is determined by the asymptotic behavior of the single-electron wave function of a free atom (or an ion). For p and d shells the overlap integrals have been calculated in Refs. [23,25,26]. Many-body effects are taken into account by choosing the Δ_j and Q parameters.

Hereafter we will be interested in the ionization of the deep shells at laser intensity higher than 10^{17} W/cm². The total ionization of the outer shells of the neutral atoms occurs in the range 10^{14} – 10^{16} W/cm² [23,24]. Therefore all atoms in the pulse front can be regarded to be ionized up to the term $l^{4l+2}(^1S_0)$. Thus the states $|l^k(\alpha SL)JM_J\rangle$ correspond to the indices f and f' , where L and S are the total orbital momentum and the spin, respectively, of the atomic shell containing k electrons with orbital momentum l ; J and M_J are the total angular momentum of the shell ($\mathbf{J} = \mathbf{L} + \mathbf{S}$) and its projection on the polarization vector of the laser radiation, respectively; α are the rest quantum numbers. In particular, $f=0$ should be understood here as the state $[[\text{Ar}^{8+}]2p^6(^1S_0)00]$, $[[\text{Kr}^{8+}]3d^{10}(^1S_0)00]$, $[[\text{Xe}^{8+}]4d^{10}(^1S_0)00]$, or $[[\text{Xe}^{18+}]4p^6(^1S_0)00]$, etc. The quantity C_f should be regarded as the ratio between the ionic concentration n_f in the state $|f\rangle$ and the concentration of neutral atoms n_{tot} in a gaseous target (or $n_0 = n_{\text{tot}}$ in the pulse front):

$$C_f(t) = n_f(t)/n_0(-\infty), \quad \sum_{f=0}^{f_{\text{tot}}} n_f(t) = n_0(-\infty).$$

The dependence of the laser intensity on the time of a laser pulse is chosen in the Gaussian form,

$$I(t) = I \exp\left[-\frac{t^2}{\tau^2} \ln 2\right], \quad (4)$$

where I is the peak intensity and τ is the FWHM. Remember that the field amplitude $F = 1$ a.u. corresponds to the intensity of linearly polarized radiation 3.51×10^{16} W/cm².

At the peak intensity of the linearly polarized laser radiation $\gtrsim 10^{16}$ W/cm² the photoelectron trajectory becomes 8-like due to the Lorentz force effect [27]. Rescattering on the parental ion will be unlikely, as is demonstrated in the experiments [1,2,4,5]. We can neglect the rescattering effects since the ions of high multiplicity (8...24) are created at the intensities from the range 10^{17} – 10^{20} W/cm². Thus, in the present work, formation of MCI's is regarded as a result of the direct impact of the laser radiation on atoms and ions.

The result of integrating the kinetic equations is a set of values $C_f(+\infty)$ corresponding to the concentrations in each ionic state after the laser-pulse completion.

It is important that the number of cascading channels grows dramatically with the increase in the ionization multiplicity. In addition, the emitted electrons may have various projections of the orbital momentum m , leading to further branching of the cascading process and, consequently, to an increase in the number of ionization channels. For example, calculation of the Kr^{17+} ion formation involves 1009 ionic states in Eqs. (1), and the number of the possible ionization channels exceeds 10^5 .

In the present work the energy levels necessary for calculations are taken from the appropriate database [28]. In the absence of these data (for krypton and xenon), the appropriate parameters are simulated using the AUTOSTRUCTURE code [29]. The output parameters $C_f(+\infty)$ are the functions of the maximum intensity in the pulse (4). The calculation results mentioned below are low-sensitive to the accuracy of the energy level positions. In particular, a level variation of 5% with respect to the result simulated by the AUTOSTRUCTURE code does not significantly change the ionization probabilities presented below in Fig. 2.

A. Ionic populations

Let the ionic charge be equal to Z . Then we obtain the population of such a charged state after pulse completion by means of summing up the appropriate populations for multiplets $|f(Z)\rangle$,

$$C(A^{Z+}, I) = \sum_{f(Z)} C_{f(Z)}(I). \quad (5)$$

For the $\text{Kr}^{9+} \dots \text{Kr}^{18+}$ ions and FWHM = 25 fs, the plots of dependence of various charged-state populations with d shell on the radiation intensity are presented in Fig. 1. The results are divided into two groups: (i) those obtained by taking into account all sequential single-electron inelastic tunneling transitions (at such FWHM the influence of the collective tunnel effect is negligibly small [25,26]) and (ii) those obtained by taking into account sequential single-electron tunneling transitions only between the ground states of the multiply charged ions (the ADK model). For ion multiplicity equal to 10 and higher, the substantial shift of the population maxima

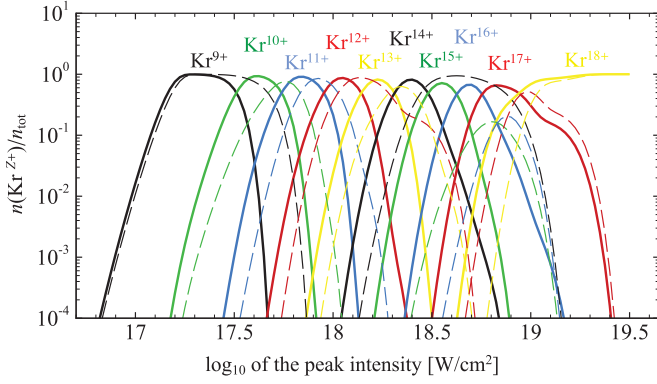


FIG. 1. (Color online) The total populations of the charged states of krypton as functions of the peak intensity of a linearly polarized laser pulse I (FWHM = 25 fs). Solid lines: the many-body model. Dashed lines: the ADK model.

and of the plot form is noted, if inelastic channels are taken into account. The possibility of the further ionization of Kr^{18+} up to the $3p$ shell is not taken into consideration.

B. Close-to-real intensity distribution

Let us calculate the MCI yield in the case of the close-to-real distribution of the laser intensity corresponding to the focused beam with the diffraction taken into account. In most experiments (see, e.g., Ref. [6]) the ions are extracted from the total focal volume rather than from its separate elements [31]. Therefore, in addition to the population, it is necessary to obtain the absolute number of ions in the given states in the focal volume.

Let us consider a focused laser beam with the Gaussian distribution of the peak intensity over the cross-section diameter,

$$I(\mathbf{r}) = I_b(z) \exp\left[-\frac{2r^2}{r_b^2(z)}\right],$$

where

$$r_b(z) = r_0[1 + (z/z_0)^2]^{1/2},$$

$$I_b(z) = I[1 + (z/z_0)^2]^{-1},$$

where r_0 is the beam waist radius, I is the peak intensity of the beam axis in the waist (the absolute intensity), z_0 is the Rayleigh range given by $z_0 = \pi r_0^2/\lambda$, and λ is the laser central wavelength. If we integrate $C(A^{Z+}, I(\mathbf{r}))$ over the beam volume, we will obtain the following integral spatially averaged ionic yield:

$$6P(A^{Z+}, I) = n_{\text{tot}} \int C(A^{Z+}, I(\mathbf{r})) d^3r = \frac{n_{\text{tot}}}{\lambda} (\pi r_0^2)^2 \times \int_0^\infty d\zeta (1 + \zeta^2) \int_0^{I/(1+\zeta^2)} C(A^{Z+}, I') \frac{dI'}{I'},$$
(6)

where $\zeta = z/z_0$. Quantity (6) defines the absolute number of Z -charged ions within the focal volume.

The relative yield of the above-listed MCI's in the beam with absolute intensity 2.6×10^{19} W/cm² is presented in Fig. 2. The experimental data are taken from Ref. [3].

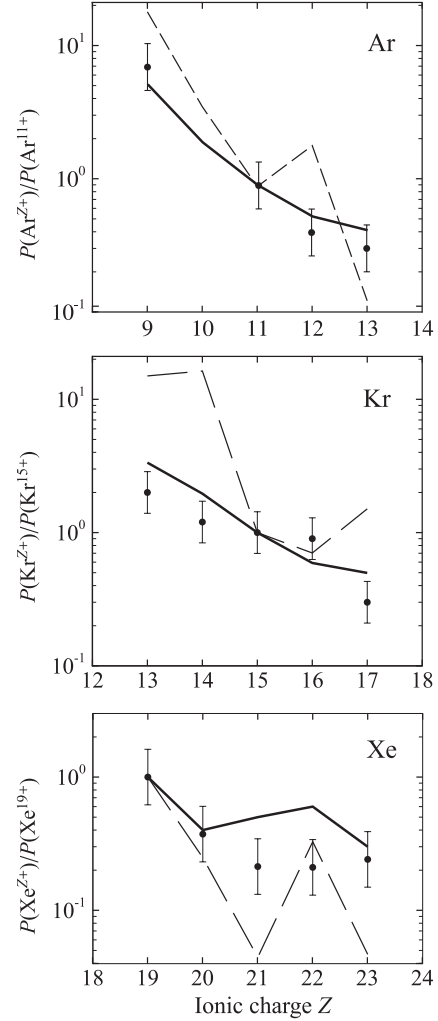


FIG. 2. The relative yield of MCI's with the given multiplicity Z in the focused Gaussian beam. The central wavelength is 800 nm; the absolute intensity is 2.6×10^{19} W/cm²; the FWHM is 25 fs. Solid lines: the many-body model. Dashed lines: the ADK model. Experimental data are taken from Ref. [3]. The experimental points shown in each figure are normalized to the calculated Ar^{11+} , Kr^{15+} , and Xe^{19+} yields, respectively, within the framework of the many-body model.

The results of calculation within the framework of the many-body ITE model agree with the experimental data for Ar ions quantitatively. For the Kr ions the theoretical results slightly exceed the limits of the experimental errors. Nevertheless, the theoretical data can be considered to be in agreement with the experimental data qualitatively. The experimental data for Xe^{21+} , Xe^{22+} , and Xe^{23+} , which appear underestimated compared to the many-body theory, can be explained by the lengthening of the trajectory of the tunnel electron motion due to relativistic distortion of this trajectory by the magnetic field. Obviously, such lengthening of the sub-barrier trajectory results in decreasing the tunneling rate. As a result, the theoretical plots in Fig. 2 for Xe^{21+} , Xe^{22+} , and Xe^{23+} ions will descend and approach the experimental values. Note that in Refs. [19,20], the nonrelativistic tunneling regime is indicated if the ionization multiplicity is $\lesssim 20$.

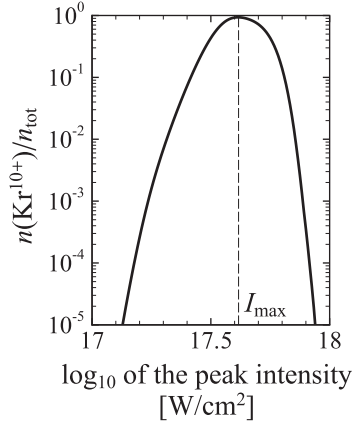


FIG. 3. The population of the Kr^{10+} charged state as a function of the peak intensity of the linearly polarized radiation with FWHM = 25 fs.

The results obtained with the single-body ADK model do not reproduce qualitatively the cited experimental data even if the absolute intensity of the pulse is regarded as a fitting parameter. Note that for the interpretation of the obtained experimental data, the authors of Ref. [3] had to change the value of the absolute intensity of laser radiation in the ADK model significantly. For example, the values $1.3 \times 10^{19} \text{ W/cm}^2$, $4.1 \times 10^{18} \text{ W/cm}^2$, and $3.5 \times 10^{18} \text{ W/cm}^2$ were taken for argon, krypton, and xenon, respectively.

Comparison with the experimental data from Ref. [5] is difficult because of the large dispersion of the experimental values.

III. DEPENDENCE OF POPULATION MAXIMUM ON IONIC CHARGE

Let us consider the dependence of the charged-state population with the specified Z on the radiation intensity I in a spatially homogeneous beam in more detail (Fig. 1). Every function (5) has its maximum at some point I_{\max} shown in Fig. 3, e.g., for the Kr^{10+} ion. In this section the dependence of I_{\max} on the ionization multiplicity Z is investigated. In Ref. [12] the empirical dependence $I_{\max} \sim Z^2$ is obtained for $\text{Xe}^{1+} \dots \text{Xe}^{25+}$ ions in the case of circular polarization of radiation by fitting this dependence to the results calculated within the framework of the ADK model by using the least-squares method. As is clear from the results mentioned in the preceding section, the ADK model describes the formation of the MCI's unsatisfactorily even qualitatively. In this section, a different approximation formula, which can be supported theoretically, is obtained. For simplicity let us consider the linearly polarized radiation and the ionization multiplicity higher than 8, when the rescattering is suppressed by the magnetic component of the laser field.

A. Three-ion ionization model

Let us estimate the dependence of I_{\max} on the ionization multiplicity Z and on the FWHM τ within the same shell. Let us consider the simplest cascading model of the successive ionization,

$$A^{(Z-1)+} \xrightarrow{W_{01}(t)} A^{Z+} \xrightarrow{W_{12}(t)} A^{(Z+1)+}, \quad (7)$$

which allows to reproduce the mechanism of the population maximum formation qualitatively. Let us designate the populations of the appropriate charged states as $C_i(t)$, $i = 0, 1, 2$, and the transition rates between them as $W_{ij}(t)$. The kinetic equations (1) for the cascade (7) take the form

$$\frac{dC_0}{dt} = -W_{01}(t)C_0(t), \quad (8)$$

$$\frac{dC_1}{dt} = W_{01}(t)C_0(t) - W_{12}(t)C_1(t),$$

$$\frac{dC_2}{dt} = W_{12}(t)C_1(t), \quad (9)$$

$$C_0(-\infty) = 1, \quad C_1(-\infty) = C_2(-\infty) = 0.$$

The set of equations (8) with initial conditions (9) is solved by quadratures. Let us give the expression for C_1 :

$$\begin{aligned} C(A^{Z+}, I) &= C_1(+\infty) \\ &= \exp \left[- \int_{-\infty}^{+\infty} W_{12}(t) dt \right] \int_{-\infty}^{+\infty} W_{01}(t) \\ &\quad \times \exp \left\{ \int_{-\infty}^t [W_{12}(t') - W_{01}(t')] dt' \right\} dt. \end{aligned} \quad (10)$$

The expressions for the transition rates (3) depending on the pulse envelope (4) have sharp maximum at $t = 0$,

$$W_{ij}(t) \approx W_{ij} \exp \left(- \frac{2F_a}{3F} \right) \exp(-t^2/\tau_*^2), \quad (11)$$

where

$$\tau_*^2 = \frac{3F}{F_a \ln 2} \tau^2, \quad (12)$$

where F is the electric field peak intensity in the laser pulse. The dependence of the preexponential factor W_{ij} on time will be neglected and considered to be equal for all transitions:

$$W_{01} \approx W_{12} \approx w.$$

Let us approximate the sharp maximum in (11) by the Dirac δ function:

$$W_{ij}(t) \approx \tau_* \sqrt{\pi} w \exp \left(- \frac{2F_a}{3F} \right) \delta(t). \quad (13)$$

The factor $\tau_* \sqrt{\pi}$ is introduced into this equation so that the integrals of functions (11) and (13) with infinite limits are equal. The dependence of the factor κ on Z in Eq. (3) is well approximated by the power law,

$$\kappa \approx \beta Z^\delta, \quad (14)$$

where $\delta \approx 1$ (Fig. 4). Thus,

$$F_a \approx \beta^3 Z^{3\delta}. \quad (15)$$

The substitution of (15) into (12) and (13) leads to the expression

$$W_{ij}(t) \approx w \tau \sqrt{\frac{3\pi F}{Z_{ij}^{3\delta} \beta^3 \ln 2}} \exp \left[- \frac{2Z_{ij}^{3\delta} \beta^3}{3F} \right] \delta(t), \quad (16)$$

where $Z_{01} = Z$, $Z_{12} = Z + 1$.

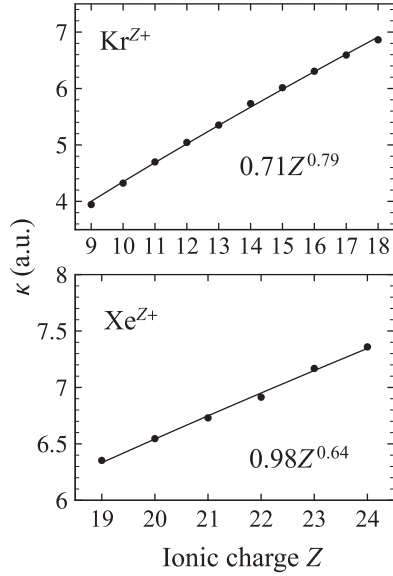


FIG. 4. The dependence of the wave number of the bound electron on the charge: bullet points show the results of the calculation using the AUTOSTRUCTURE code; solid line corresponds to the dependence (14) fitted by the least-squares method.

Substituting (16) into (10) and assuming that $Z \gg 1$ gives

$$C(A^{Z+}, I) \approx 2\zeta \exp\left\{-\zeta \left[\left(1 - \frac{3\delta}{2Z}\right) e^{-3\delta\xi^2/Z} + 1 \right]\right\}, \quad (17)$$

where

$$\xi^2 = \frac{2Z^{3\delta}\beta^3}{3F} \gg 1, \quad \zeta = w\tau \sqrt{\frac{\pi \ln 2}{2}} \frac{e^{-\xi^2}}{\xi}. \quad (18)$$

Based on the first inequality (18), the first factor in the square brackets (17) can be neglected leading to the quite simple function

$$C(A^{Z+}, I) \approx 2\zeta e^{-\zeta},$$

approaching maximum at

$$\zeta = \zeta_{\max} = 1. \quad (19)$$

As can be seen from (18), the quantity ζ substantially depends on the ξ parameter. In order to provide fulfillment of (19) with arbitrary F and Z relating to the same shell, the quantity $\xi = \xi_{\max}$ must be kept constant. This implies the desired relation,

$$I_{\max} = \gamma Z^{6\delta}. \quad (20)$$

The $C(A^{Z+}, I_{\max})$ values can be obtained as a result of the numerical solution of the complete set of kinetic equations (1). Thereafter, the value of the γ constant is obtained as the result of fitting by the least-squares method. Let us note that the exponent in (20) does not depend on the pulse FWHM and the polarization of radiation. These parameters affect the value of constant γ only.

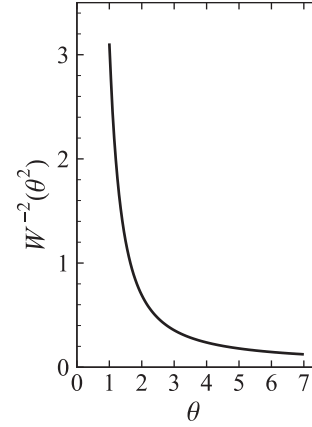


FIG. 5. The plot of $W^{-2}(\theta^2)$.

The $I_{\max}(\tau)$ dependence is also of interest. It is obtained on the basis of (18) from the solution of the transcendental equation with the τ parameter,

$$w\tau \sqrt{\frac{\pi \ln 2}{2}} \frac{e^{-\xi^2}}{\xi} = 1,$$

and is given by the Lambert W function [32]:

$$\xi_{\max}^2 = \frac{1}{2} W[(w\tau)^2 \pi \ln 2]. \quad (21)$$

Now the estimation (20) is generalized in terms of (21) in the following way:

$$I_{\max} = \tilde{\gamma} Z^{6\delta} W^{-2}[(w\tau)^2 \pi \ln 2],$$

where $\tilde{\gamma}$ is the a τ -independent constant.

Let us consider the limiting cases of this formula. For short pulses ($w^2\tau^2 \ll 1$),

$$I_{\max} \sim Z^{6\delta} (w\tau)^{-4}.$$

For long pulses ($w^2\tau^2 \gg 1$),

$$I_{\max} \sim Z^{6\delta} \left[\ln z - \ln \ln z - \frac{\ln \ln z}{\ln^2 z} - \frac{\ln \ln z}{\ln z} + \frac{\ln^2 \ln z}{2 \ln^2 z} \right]^{-2},$$

where $z = (w\tau)^2 \pi \ln 2$.

At decreasing FWHM τ the positions of maxima shift monotonically to increasing intensities. The plot of dependence of the maximum position on the parameter $\theta \sim \tau$ is presented in Fig. 5.

B. Comparison of different parametrizations of $I_{\max}(Z)$ dependence

Let the set of maximums I_i corresponding to N successive ionization multiplicities Z_i within the same shell ($i = 1, 2, \dots, N$) be obtained by the numerical integration of (1). Let us choose

$$I_{\text{approx}} = \gamma Z^k \quad (22)$$

as an approximation formula containing γ and k parameters. For comparison between the I_i exact values and their approximate values (22) the least-squares method in the logarithmic

scale is used. Let us create the defect of approximation in the following form:

$$\rho_I^2(k, \gamma) = \frac{1}{N} \sum_{i=1}^N \log_{10}^2 (\gamma Z_i^k / I_i). \quad (23)$$

After minimization of (23) over γ at fixed k we obtain

$$\log_{10} \gamma = [\log_{10} I] - k[\log_{10} Z], \quad (24)$$

where

$$[x] \equiv \frac{1}{N} \sum_{i=1}^N x_i$$

is the Gaussian symbol for the arithmetical mean.

Expression (23) is calculated for γ derived from (24) for three different k values. In the first case, the value of k is determined numerically giving the unconstrained minimum of the defect (23). This k value will be called optimal. It will correspond to the best approximation in the form of (22). In the second case it is assumed that $k = 2$ according to Ref. [12]. Finally, in the third case it is assumed that $k = 6\delta$, which was obtained in Sec. III A. Let us remember that parameter δ arises as a result of the wave number κ approximation by Eq. (14).

Suppose the sequence of exact values κ_i corresponds to the ionization multiplicities Z_i . The parameters β and δ will be determined by the least-squares method. Let us create the approximation defect as follows,

$$\rho_\kappa^2(\delta, \beta) = \frac{1}{N} \sum_{i=1}^N (\beta Z_i^\delta - \kappa_i)^2, \quad (25)$$

and find its constrained minimum over β at the given δ ,

$$\beta = [Z^\delta \kappa] / [(Z^\delta)^2]. \quad (26)$$

After the substitution of (26) into (25) the approximation defect will depend only on δ . Its unconstrained minimum is found numerically with respect to δ .

For estimation of approximation (22) at different k values let us compare the approximation defect values ρ_I . The results of analysis of different parametrizations (22) are given in Table I. The plots of dependences (14) and (22) for the krypton and xenon ions are shown in Fig. 6. Evidently, the value $k = 6\delta$ slightly impairs the quality of the approximation (22). For example, for the $\text{Kr}^{9+} \dots \text{Kr}^{17+}$ ions, the approximation defect at $k = 6\delta$ appears to be three times as much as at the optimal k value. At the same time both above-mentioned methods of approximation give approximately identical accuracy for the $\text{Xe}^{19+} \dots \text{Xe}^{23+}$ ions. It is explained by the higher charge of

TABLE I. Parameters of approximation (22).

| Ions | $\text{Kr}^{9+} \dots \text{Kr}^{17+}$ | $\text{Xe}^{19+} \dots \text{Xe}^{23+}$ |
|-----------------|--|---|
| The optimal k | $1.58 \times 10^{12} Z^{5.44}$ | $9.71 \times 10^{12} Z^{4.03}$ |
| ρ_I | 0.028 | 0.013 |
| $k = 6\delta$ | $8.48 \times 10^{12} Z^{4.74}$ | $1.90 \times 10^{13} Z^{3.84}$ |
| ρ_I | 0.068 | 0.015 |
| $k = 2$ | $9.04 \times 10^{15} Z^2$ | $4.67 \times 10^{15} Z^2$ |
| ρ_I | 0.306 | 0.061 |

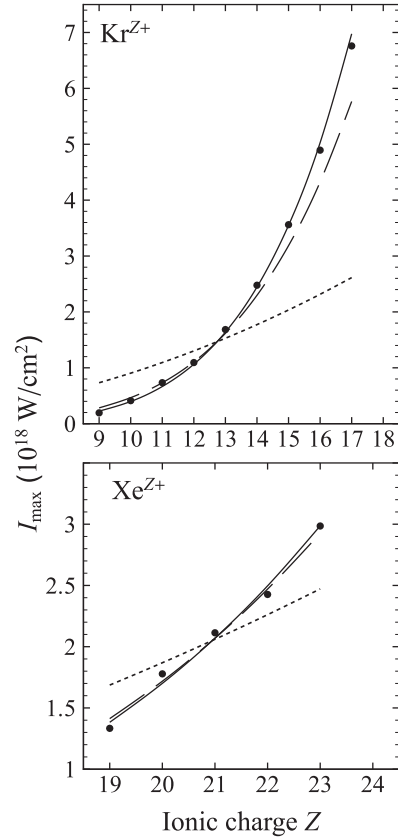


FIG. 6. The dependence of population maximum values I_{\max} on ionic charge Z for the $\text{Kr}^{9+} \dots \text{Kr}^{17+}$ and $\text{Xe}^{19+} \dots \text{Xe}^{23+}$ ions. Bullet points correspond to the results of numerical integration of the kinetic equation set (1) taking into account many-body effects. Continuous lines correspond to the approximation (22) with different k values. Solid line corresponds to the optimal k value; dashed line corresponds to $k = 6\delta$, and the δ parameter is derived from Eq. (14); dotted line corresponds to $k = 2$. See explanations in Table I.

the xenon ions, for which the exponent in Eq. (3) appears to be effectively higher with respect to the module than in case of the krypton ions. As a consequence, approximation (13) appears to be more reasonable for xenon than for krypton. The difference between these two ways of approximation is due to, on the one hand, the error under assumption (16) and on the other hand, neglecting the rest channels excluded from the three-ion model (inelastic tunneling, etc.).

The approximation parameter value $k = 2$ gives the value of defect an order of magnitude higher compared to the above-mentioned approximation methods. At the same time, using $k = 2$ appears to be efficient for Z referring to the different shells of the same ion [12].

IV. CONCLUSIONS

The performed calculations demonstrate that the computed yield of $\text{Ar}^{9+} \dots \text{Ar}^{13+}$ ions agrees with experimental data quantitatively. The results of $\text{Kr}^{13+} \dots \text{Kr}^{17+}$ ion formation probability calculations are on the borders of experiment errors. This can be considered as the qualitative agreement between theory and experiment. Theoretical data for

$\text{Xe}^{21+} \dots \text{Xe}^{23+}$ ion formation lie above experimental values, and the disagreement increases with the ion multiplicity growth. In principle, this disagreement may be due to the non-relativistic approximation in our theory. Taking into account relativistic effects should result in decreasing the probability of high multiplicity ion formation. This conclusion is based on the fact that the relativistic effects distort the sub-barrier electron trajectory. As a result, the trajectory lengths and the tunneling probability decreases [19,20]. We note that in case this assumption is confirmed by relativistic calculations, this would mean that in a superstrong light field the relativistic effects for tunnel ionization become significant at ionization multiplicity higher than 20. This multiplicity is much lower than a typical relativistic nuclear charge equal to the inverse

value of the fine-structure constant, $Z^* = \alpha^{-1} \approx 137$. We should also pay attention to the fact that single-body ADK theory significantly disagrees with the experimental data in all cases.

The proposed simple parametrization of population maximum position dependence on ionization multiplicity and laser pulse duration well reproduces the results of direct numerical calculations.

ACKNOWLEDGMENTS

This research was supported by the Russian Foundation for Basic Research (Grant No. 11-02-00170). Authors thank K. Yamakawa for helpful discussions.

-
- [1] E. A. Chowdhury, C. P. J. Barty, and B. C. Walker, *Phys. Rev. A* **63**, 042712 (2001).
- [2] M. Dammasch, M. Dörr, U. Eichmann, E. Lenz, and W. Sandner, *Phys. Rev. A* **64**, 061402 (2001).
- [3] K. Yamakawa, Y. Akahane, Y. Fukuda, M. Aoyama, N. Inoue, and H. Ueda, *Phys. Rev. A* **68**, 065403 (2003).
- [4] E. Gubbini, U. Eichmann, M. P. Kalashnikov, and W. Sandner, *J. Phys. B* **38**, L87 (2005).
- [5] K. Yamakawa, Y. Akahane, Y. Fukuda, M. Aoyama, N. Inoue, H. Ueda, and T. Utsumi, *Phys. Rev. Lett.* **92**, 123001 (2004).
- [6] E. Gubbini, U. Eichmann, M. P. Kalashnikov, and W. Sandner, *Phys. Rev. Lett.* **94**, 053602 (2005).
- [7] W. A. Bryan *et al.*, *Nature Phys.* **2**, 379 (2006).
- [8] S. Palaniyappan, A. DiChiara, I. Ghebregziabher, E. L. Huskins, A. Falkowski, D. Pajeroski, and B. C. Walker, *J. Phys. B* **39**, S357 (2006).
- [9] E. Gubbini, U. Eichmann, M. Kalashnikov, and W. Sandner, *J. Phys. B* **39**, S381 (2006).
- [10] A. D. DiChiara, I. Ghebregziabher, R. Sauer, J. Waesche, S. Palaniyappan, B. L. Wen, and B. C. Walker, *Phys. Rev. Lett.* **101**, 173002 (2008).
- [11] A. D. DiChiara *et al.*, *Phys. Rev. A* **81**, 043417 (2010).
- [12] N. I. Shvetsov-Shilovski, A. M. Sayler, T. Rathje, and G. G. Paulus, *Phys. Rev. A* **83**, 033401 (2011).
- [13] G. Mourou, T. Tajima, and S. V. Bulanov, *Rev. Mod. Phys.* **78**, 309 (2006).
- [14] P. B. Corkum, *Phys. Rev. Lett.* **71**, 1994 (1993).
- [15] L. V. Keldysh, *Sov. Phys. JETP* **20**, 1307 (1965).
- [16] B. M. Smirnov and M. I. Chibisov, *Sov. Phys. JETP* **22**, 585 (1966).
- [17] A. M. Perelomov, V. S. Popov, and M. V. Terentev, *Sov. Phys. JETP* **23**, 924 (1966).
- [18] M. V. Ammosov, N. B. Delone, and V. P. Krainov, *Sov. Phys. JETP* **64**, 1191 (1986).
- [19] N. Milosevic, V. P. Krainov, and T. Brabec, *Phys. Rev. Lett.* **89**, 193001 (2002).
- [20] V. S. Popov, B. M. Karnakov, V. D. Mur, and S. G. Pozdnyakov, *Sov. Phys. JETP* **102**, 760 (2006).
- [21] B. A. Zon, *Sov. Phys. JETP* **89**, 219 (1999).
- [22] B. A. Zon, *Sov. Phys. JETP* **91**, 899 (2000).
- [23] A. S. Kornev, E. B. Tulenko, and B. A. Zon, *Phys. Rev. A* **68**, 043414 (2003).
- [24] A. S. Kornev, E. B. Tulenko, and B. A. Zon, *Phys. Rev. A* **69**, 065401 (2004).
- [25] A. S. Kornev, E. B. Tulenko, and B. A. Zon, *Phys. Rev. A* **79**, 063405 (2009).
- [26] A. S. Kornev, E. B. Tulenko, and B. A. Zon, *Sov. Phys. JETP* **111**, 921 (2010).
- [27] L. D. Landau, and E. M. Lifshitz, *The Classical Theory of Fields* (Pergamon, Oxford, 1991).
- [28] Yu. Ralchenko, A. E. Kramida, J. Reader, and NIST ASD Team, *NIST Atomic Spectra Database (version 3.1.5)* [online]. Available at: <http://physics.nist.gov/asd3> [2011/11/16 22:41:20]. (National Institute of Standards and Technology, Gaithersburg, MD, 2008).
- [29] [<http://amdpp.phys.strath.ac.uk/autos/>].
- [30] P. Lambropoulos, K. G. Papamihail, and P. Declava, *J. Phys. B* **44**, 175402 (2011).
- [31] M. A. Walker, P. Hansch, and L. D. Van Woerkom, *Phys. Rev. A* **57**, R701 (1998).
- [32] N. G. de Bruijn, *Asymptotic Methods in Analysis* (North-Holland, Amsterdam, 1958); [<http://dlmf.nist.gov/4.13>].